Orientational Ordering of a Bent-Core Mesogen by Two-Dimensional ^{13}C NMR Spectroscopy

J. Xu,[†] K. Fodor-Csorba,[‡] and Ronald Y. Dong*[,†,§]

Department of Physics and Astronomy, University of Manitoba, Winnipeg, MB, Canada R3T 2N2, Research Institute of Solid State Physics and Optics, Konkoly Thege u. 29−33, Budapest, Hungary, and Department of Physics and Astronomy, Brandon University, Brandon, MB, Canada R7A 6A9

Received: September 24, 2004; In Final Form: December 17, 2004

Various two-dimensional (2D) NMR techniques are reported on a bent-core mesogen 4,6-dichloro-1,3-phenylenebis[4′-(9-decenyloxy)-1,1′-biphenyl] carboxylate in its nematic and solid phases in order to unambiguously assign its carbon-13 NMR spectrum. The ^{13}C chemical shifts from the molecular core were studied as a function of temperature to extract its molecular geometry and orientational order tensor. To this end, the chemical shift anisotropy tensors of some carbon sites were measured in the solid state of this mesogen using a recent method called the separation of undistorted powder patterns by effortless recoupling (SUPER). The average bending angle subtended by the two arms of the bent-core structure is determined to be 148.7°. The C−H dipolar couplings obtained from the separated local field (SLF) experiment for the aromatic rings are used to find the local order parameter tensors.

Introduction

Multidimensional NMR experiments have been carried out in liquid crystals[1,2] consisted of molecules having various anisometric shapes so as to elucidate the structure and orientational ordering. Among them, bent-core (or boomerang-shaped) mesogens[3−5] have recently attracted much attention, partly due to the observation of chirality in tilted smectic phases (the so-called B-phases) formed by these achiral molecules, and the associated electrooptical switching properties,[6] and partly due to the scientific curiosity in phenomena such as biaxial nematic phases in low-molecular-mass thermotropic systems.[7−9] Chirality attributable to a twisted conformation has also been reported in B-phases.[10] There are several ^{13}C NMR papers reported in the last few years[10−16] on bent-core (banana) mesogens. These studies have revealed that analyses of ^{13}C spectra need the proper carbon peak assignments, as well as the knowledge of chemical shift anisotropy (CSA) tensor and its orientation for each carbon in the molecule in order to extract the molecular geometry and/or the order parameters. As a partial solution to the lack of precise CSA tensors, other nuclei such as ^{1}H,[7] ^{2}H,[16] and ^{19}F[17] were used to support the ^{13}C NMR results. Here an alternative solution is explored, which involves doing two-dimensional (2D) ^{13}C NMR on bent-core mesogens in order to aid the spectral assignment and to determine C−H dipolar couplings as well as the principal elements of CSA tensors.

The six parameters of a CSA tensor (three principal values and three Euler angles specifying the principal axis system in a crystal-fixed frame) can be obtained by means of single crystal measurements.[18] To grow single crystals of sufficient size for banana mesogens may be a daunting task. However, the principal values of a CSA tensor can be determined quite reliably from the magic-angle-spinning (MAS) sideband pattern.[19,20] For systems with many carbon sites, the sideband manifolds from different sites overlap, making the analysis quite difficult. Various 2D NMR schemes have been designed to separate the isotropic and anisotropic chemical shift information.[21−25] All these methods retain CSA information while obtaining a clear distinction between the different carbon sites. Recently, a 2D phase adjusted spinning sideband (2D-PASS) experiment[24,25] has shown a number of advantages over the previous 2D schemes. However, most of the known sideband-separation techniques are performed at unusually low sample rotation frequencies ($f_{rot} < 2$ kHz).

The CSA of a carbon site produces a characteristic powder pattern in nonrotating solids, with a peak at its principal element δ_{22}, the middle value in the CSA tensor, and sharp steps at the two other principal components. Such powder patterns have the advantage of giving the magnitudes of the principal components of CSA tensor directly either with or without spectral simulations. However, they do not give the CSA principal axes in relation to a particular molecule axis. A recent method for rotating solids, termed the separation of undistorted powder patterns by effortless recoupling (SUPER), was proposed[26] to obtain CSA powder patterns using suitably rotation-synchronized radio frequency (rf) pulses. This has produced a number of ^{13}C powder spectra in organic solids and polymers for different chemical (aromatic, unprotonated sp^2-hybridized, and aliphatic) sites. Here the SUPER method is employed in the solid phase of a banana mesogen, 4,6-dichloro-1,3-phenylenebis-[4′-(9-decenyloxy)-1,1′-biphenyl] carboxylate (10DClPBBC). When one is comparing these values with typical principal values of CSA tensors from model compounds, this method may be used to aid the spectral assignment of ^{13}C spectrum in the isotropic phase of banana mesogens. 10DClPBBC has recently been studied[15] by ^{13}C NMR to obtain the order parameters in its nematic phase. However, the results were based on the analyses of the ^{13}C chemical shifts of the biphenyl fragments, and the assumption of their para axes making an angle of 11.8° with the long molecular axis, a value obtained in a similar banana molecule.[16] The present study has removed such a crude

[†] University of Manitoba.
[‡] Research Institute of Solid State Physics and Optics.
[§] Brandon University.

10.1021/jp045644y CCC: $30.25
Published on Web 02/12/2005

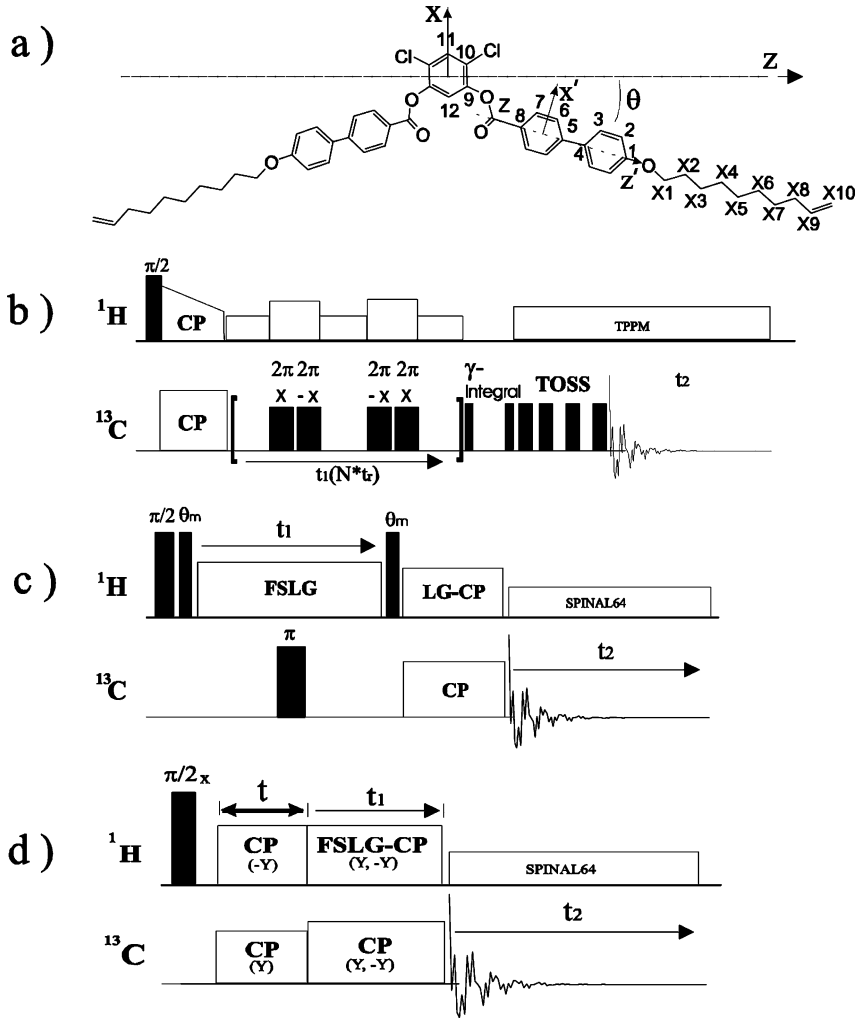

Figure 1. (a) Molecular structure of 10DClPBBC, (b) 2D SUPER pulse sequence, (c) carbon−proton HETCOR pulse sequence using FSLG homonuclear decoupling, and (d) SLF pulse sequence modified by including the cross-polarization inversion.

assumption, since the central phenyl ring can now be studied using the CSA results from the SUPER experiment.

2D carbon−proton (HETCOR) chemical shift correlation spectroscopy has been used in solids[27−29] under MAS to assign spectra. For aligned liquid crystals, MAS is not required (and is not desirable) to obtain a good spectral resolution. This is used here on the stationary sample of 10DClPBBC. Both homonuclear and heteronuclear dipolar decoupling must, however, be used during the evolution t_1 and acquisition t_2 periods, respectively. 2D separated local field (SLF) NMR spectroscopy has been used to measure and assign C−H dipolar couplings.[30−32] In the SLF method, a ^{13}C spin evolves under the influence of dipolar local fields produced by the surrounding protons. Its variant is the proton-detected local field (PDLF) technique, in which the spectra are governed by simple two-spin interactions, resulting in a higher spectral resolution.[33−37] In the present study, both SLF and PDLF experiments were carried out at a single temperature in the nematic phase of 10DClPBBC. Only the SLF spectrum is reported here to aid the spectral assignment, and to obtain C−H dipolar couplings. These C−H couplings enable the determination of local order parameter tensors for the biphenyl rings.

The present study reports on how 2D ^{13}C NMR techniques may be used to complement the 1D ^{13}C spectroscopy, and how ^{13}C NMR can become a stand-alone method for elucidating structure and orientational ordering of banana mesogens. It also shows that expensive syntheses of partially deuterated compounds may be avoided.[16]

Experimental Section

The structure of 10DClPBBC is sketched in Figure 1a, showing the carbon labels. The synthesis and its characterization were reported elsewhere.[38] The phase transition temperatures observed by polarization microscopy are

$$\text{crystal}_1 \xleftrightarrow[51.9\,^\circ\text{C}]{} \text{crystal}_2 \xleftrightarrow[72.7\,^\circ\text{C}]{} \text{crystal}_3 \xleftrightarrow[87.6\,^\circ\text{C}]{} \text{N} \xleftrightarrow[98.8\,^\circ\text{C}]{} \text{I}$$

and the clearing temperature (T_C) determined by NMR is 373.5 K. The ^{13}C NMR experiments were carried out at 100.6 MHz with a Bruker Avance 400 spectrometer. The 1D and 2D ^{13}C NMR spectra of the banana sample in $CDCl_3$ were reported previously.[15] The ^{13}C NMR experiments of the static neat sample were carried out with a 2-channel HX solid probe. The sample was macroscopically aligned within the superconducting magnet by cooling slowly from the isotropic phase. The ^{13}C spectrum in the isotropic phase was collected by a carbon 90° pulse together with Waltz-16 proton decoupling. The ^{13}C spectra in the nematic phase were collected[15] using standard CP (cross-polarization) for 2 ms after the 90° proton irradiation. The ^{1}H 90° pulse width was 3.4 μs. Proton decoupling during the ^{13}C signal acquisition was achieved by SPINAL-64 pulse sequence[39] with a minimal decoupling field of ca. 10 kHz. To avoid sample

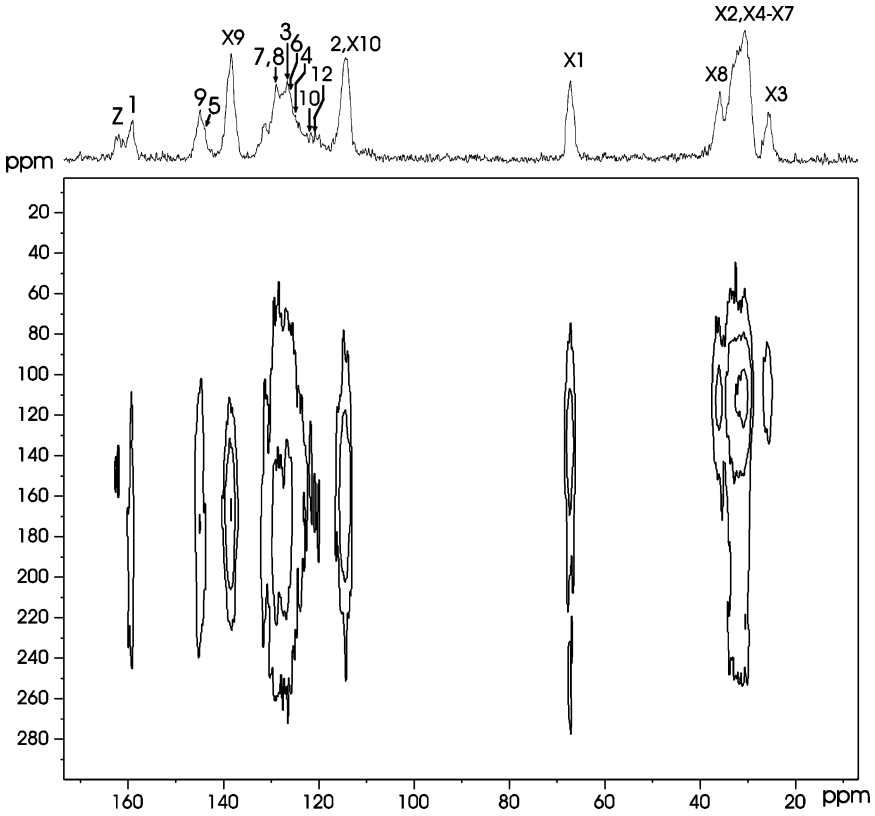

Figure 2. 2D SUPER spectrum in the solid phase of 10DClPBBC at room temperature and at a spinning rate of 4.9 kHz using the pulse sequence in Figure 1b.

heating, the recycle delay between each FID acquisition was 6 s. The temperature calibration was made for a given air flow using the known phase transition temperatures of a liquid crystal. The temperature gradient across the sample was estimated to be within 0.3 deg. The ^{13}C peak assignments in the aligned sample are those given before[15] but with only a minor revision (see below). The 2D ^{13}C SUPER was performed in the solid state of 10DClPBBC at room temperature and at a spinning speed (f_{rot}) of 4.9 kHz using a 4 mm double resonance CP/MAS probe. The experiment, which correlates CSA powder patterns in the f_1 dimension with the isotropic chemical shifts in the f_2 dimension, is based on the experiment of Tycko, Dabbagh and Mirau,[40] but can provide a better compensation for experimental imperfections such as inhomogeneous rf (B_1) fields. The scaling factor is also more favorable. Its pulse sequence is shown in Figure 1b. After a ramp CP of 2 ms, four ^{13}C 2π pulses are used to recouple CSA during MAS. The ^{13}C power level required for recoupling is $f_{rf} = 12.12 \times f_{rot}$. To avoid the signal being dephased by strong heteronuclear couplings during the recoupling 2π pulses, a cw proton decoupling field of 192 kHz is applied. The spinning sidebands are removed by the γ integral[41] and TOSS (the γ integral is needed in the 2D MAS experiments). During acquisition, TPPM15 decoupling sequence is applied at a decoupling level of 147 kHz. The number of t_1 increments was 32 with 192 scans per t_1 increment, and the States-TPPI[42] quadrature detection method was used. The scaling factor for CSA was set at 0.155.

2D carbon−proton HETCOR spectroscopy was carried out on the static sample using the pulse sequence shown in Figure 1c. The π pulse in the carbon channel is to refocus the dipolar coupling while leaving the evolution of the proton offset (chemical shift) unaffected. Homonuclear decoupling of the abundant spins during t_1 is achieved by the frequency-switched Lee−Goldburg (FSLG-2),[43] a variant of the off-resonance "magic angle cw" irradiation proposed by Lee and Goldburg.[44] Here the proton rf irradiation is switched between the two LG conditions $\pm\gamma B_1/\sqrt{2}$ for each 2π rotation of the proton magnetization about the effective field. The scaling factor of FSLG-2 decoupling sequence for the chemical shift is 0.578. The first magic angle (θ_m) pulse applied after the proton 90° pulse puts the proton transverse magnetization perpendicular to the effective field, and the second magic angle pulse after the FSLG sequence puts them back onto the $x-y$ plane. LG and CP are used simultaneously to establish selective heteronuclear polarization transfer during the cross-polarization. Generally, the Hartmann−Hahn matching condition during LG-CP was found to be very sensitive. A phase sensitive spectrum using the STATES method was obtained. The 2D SLF NMR spectrum was obtained at 351 K on the stationary sample using the pulse sequence shown in Figure 1d. The dipolar oscillations were observed on the CP buildup curves when homonuclear decoupling using FSLG-2 at 53.2 kHz was applied during CP. The LG decoupling during t_1 produced a theoretical scaling factor of $\sin \theta_m = 0.82$ for the dipolar oscillation (not accounted for in getting the SLF spectrum). During t_2, heteronuclear decoupling was achieved by SPINAL-64 at 42.3 kHz. To decrease the central peaks in the 2D SLF spectrum, cross-polarization inversion[45,46] for a fixed duration (2 ms) was also included in the pulse sequence. The number of t_1 increments was 80 with 96 scans per t_1 increment, and the STATES method was used. Typical proton and carbon 90° pulse widths in 2D experiments were ca. 2 μs and 2.8 μs, respectively.

Results and Discussion

The 2D SUPER spectrum in the solid phase of 10DClPBBC is shown in Figure 2, together with the 1D isotropic spectrum (f_2 projection) and ^{13}C peak assignments at the top. The CSA

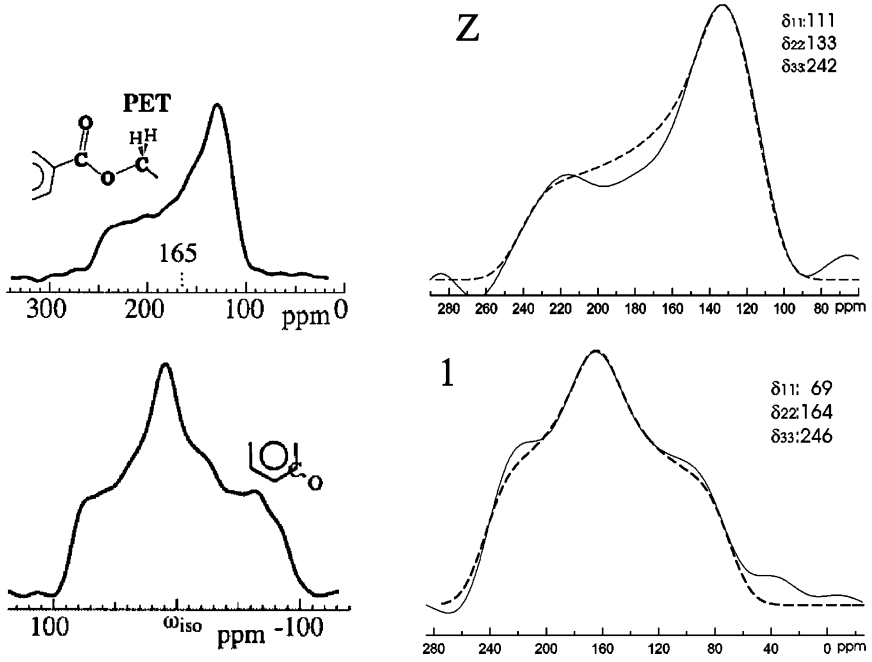

Figure 3. Plots of f_1 slices from the 2D SUPER spectrum for carbon sites 1 and *Z*. The powder spectra on the left column are for poly(ethylene terephthalate) (PET) (top spectrum) and 3-methoxy benzamide (bottom spectrum), which are reproduced from ref 26 for direct comparison. Dashed curves denote theoretical simulations of CSA powder patterns.

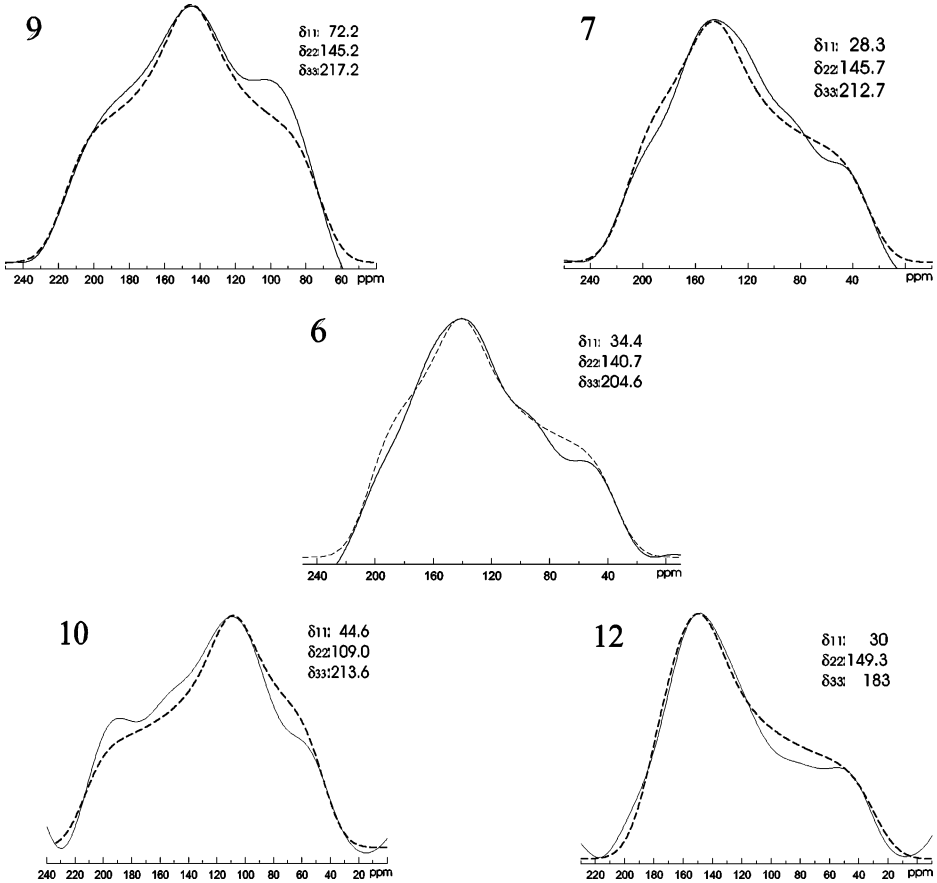

Figure 4. Same as Figure 3 for carbon sites 6, 7, 9, 10, and 12. Dashed curves denote theoretical simulations of CSA powder patterns.

powder patterns of various carbon sites from the f_1 slices of Figure 2 are shown in Figures 3 and 4. The powder line shapes were simulated using WSOLIDS1 simulation package[47] to determine the principal components of the CSA tensor, and they are shown as dashed curves in these figures. The CSA results are summarized in Table 1. In Figure 3, the observed carbon powder patterns for sites 1 and *Z* in the literature[26] are also included for direct comparisons. On the basis of this figure, the previous ^{13}C assignment in the isotropic phase[15] for sites 1 and *Z* must be reversed. Fortunately this minor modification has not significantly changed the conclusions drawn previously. The HETCOR spectrum in the nematic phase (≈78 °C) of 10DClPBBC is shown in Figure 5, which correlates the carbon and proton chemical shifts in the f_2 and f_1 dimensions. Again

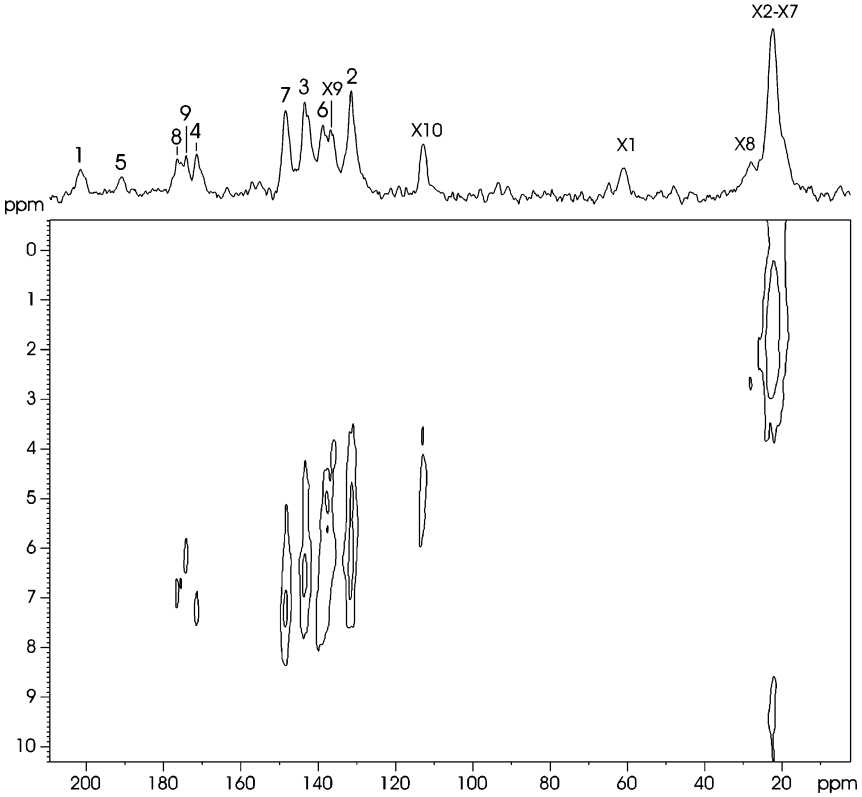

Figure 5. 2D carbon−proton HETCOR spectrum in the nematic phase of 10DClPBBC at 78 °C using the pulse sequence of Figure 1c.

TABLE 1: CSA Tensors for Various Carbon Sites (Site Labels Are for Both *Lateral* Wings) Determined by SUPER[a]

sites	1	6	7	9	10	12	*Z*
δ_{11}	69	34.4	28.3	72.2	44.6	30	111
δ_{22}	164	140.7	145.7	145.2	109	149.3	133
δ_{33}	246	204.6	212.7	217.2	213.6	183	242
δ_{iso}	159.7	126.4	128.9	144.9	122.4	120.8	162

[a] The accuracy of the δ_{ii} values is around ±2 ppm.

the 1D carbon spectrum is displaced at the top of this 2D map, together with peak assignments. The spectrum of SLF experiment, collected at 78 °C, is shown in Figure 6, in which the f_2 dimension shows the normal proton-decoupled ^{13}C peaks (top trace), while the slices in the f_1 dimension show the individual ^{13}C nuclei with the C−H dipolar couplings. Figure 7 shows some selected f_1 slices from the aromatic region. The dipolar oscillation frequencies seen in the t_1 dimension (as a function of CP time) for carbons 2,3,6 and 7 are seen to be similar, and are larger than those of the quaternary carbons 4, 5, 8, and 9. The observations are consistent with the ^{13}C peak assignments given previously.[15] The temperature-dependent chemical shifts $\delta^{(j)}$ for the aromatic region and X9 and X10 of 10DClPBBC are reproduced[15] in Figure 8.

The chemical shift δ of a carbon in a liquid crystalline phase is related to its isotropic chemical shift δ_{iso}, the components of the chemical shift tensor δ_{ij}, and local order parameter tensor S_{ij} according to[48]

$$\delta = \delta_{iso} + \frac{2}{3}S_{zz}\{\delta_{zz} - (\delta_{xx} + \delta_{yy})/2\} + \frac{1}{3}(\delta_{xx} - \delta_{yy})(S_{xx} - S_{yy}) + \frac{2}{3}(S_{yz}\delta_{yz} + S_{xz}\delta_{xz} + S_{xy}\delta_{xy}) \quad (1)$$

Neglecting S_{xy}, S_{yz}, and S_{xz}, which are usualy small, the chemical shifts $\delta^{(j)}$ of carbons on the biphenyl fragments and center ring

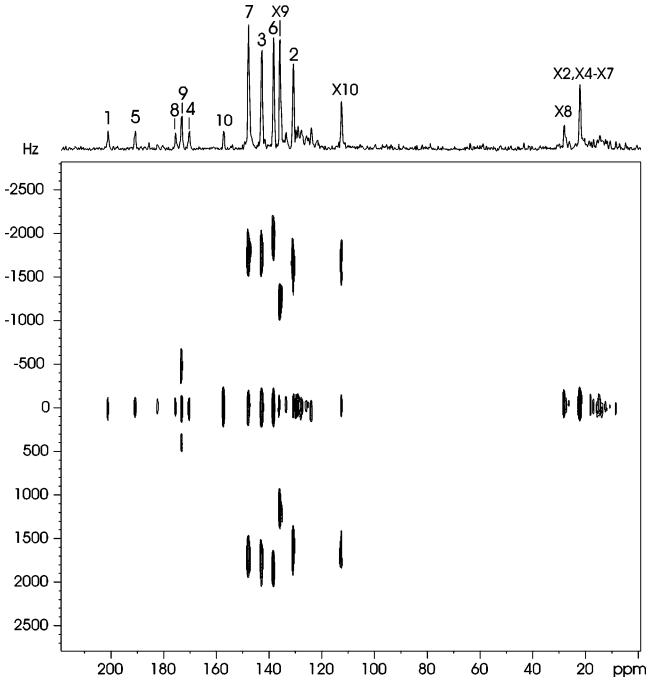

Figure 6. 2D SLF spectrum in the nematic phase of 10DClPBBC at 78°C using the pulse sequence of Figure 1d.

can be calculated separately using different local order parameter tensors:[15,16,48]

$$\delta^{(j)} = \delta_{iso}{}^{(j)} + \frac{2}{3}S_{Z'Z'}\left[P_2(\cos\beta^{(j)})(\delta_{33}{}^{(j)} - \delta_{22}{}^{(j)}) + \frac{1}{2}(\delta_{22}{}^{(j)} - \delta_{11}{}^{(j)})\right] + \frac{1}{3}(S_{X'X'} - S_{Y'Y'})[\cos^2\beta^{(j)}\delta_{22}{}^{(j)} + \sin^2\beta^{(j)}\delta_{33}{}^{(j)} - \delta_{11}{}^{(j)}] \quad (2)$$

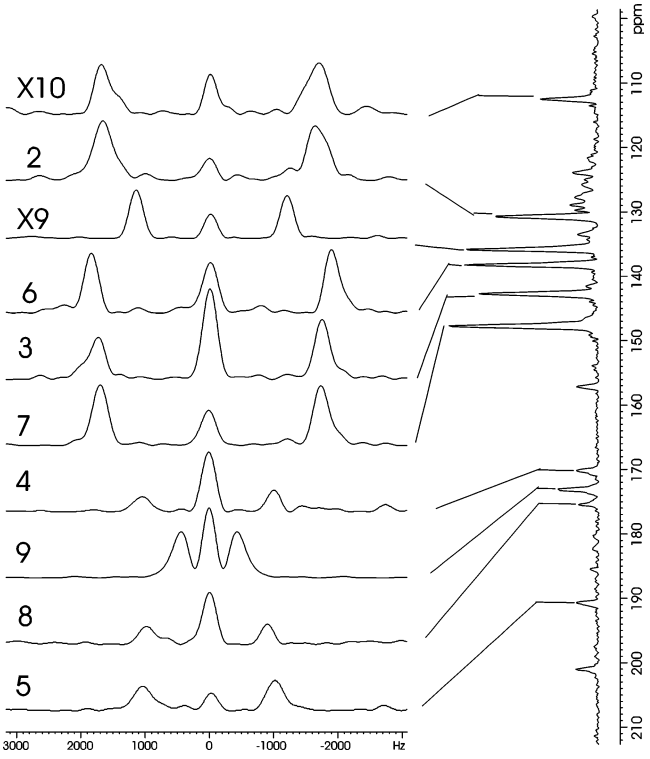

Figure 7. Plots of 1D slices in the f_1 dimension of Figure 6 for some protonated carbon sites.

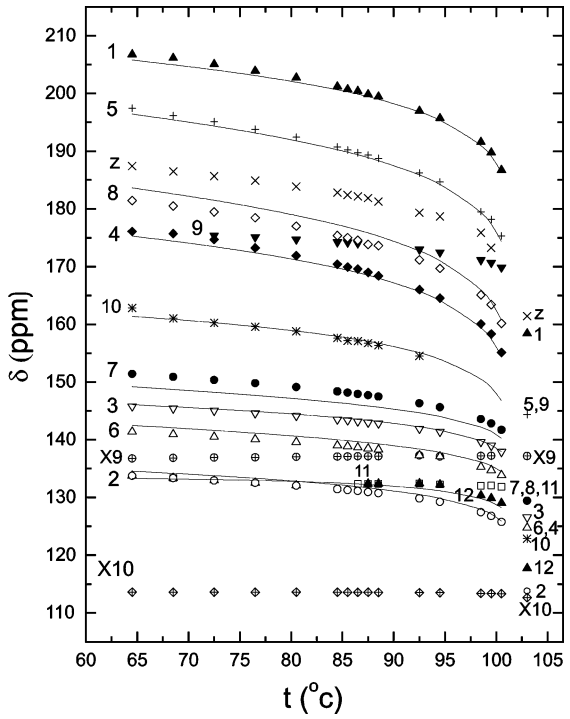

Figure 8. Plots of chemical shifts for the aromatic carbons and aliphatic carbons X9 and X10 in the isotropic and nematic phases of 10DClPB-BC. The carbon labels are indicated in Figure 1a. Solid curves denote calculated chemical shifts after a global minimization.

where $\beta^{(j)}$ is the angle between the principal direction of $\delta_{33}^{(j)}$ in the $\delta^{(j)}$ tensor for the jth carbon and the z' axis of the local (x', y', z') frame fixed on a molecular fragment. To distinguish the two local frames, we have chosen the (x, y, z) frame fixed on the central ring fragment, with the z axis along the direction joining the chlorine atoms. The other local (x', y', z') frame is fixed on a biphenyl fragment, where the z' axis is along the ring para axes and the x' axis is on a biphenyl ring plane. As seen below, the local order parameter S_{zz} of the central ring reflects the nematic order parameter of the molecule. The CSA tensors used in the present study are those given in Table 1 (from SUPER) and literature values reproduced in Table 2.[49−51] The principal axis system (1, 2, 3) for the chemical shift tensor is chosen by assuming that the 3 axis is along the C−H bond, or C−C bond, and the 1 axis is normal to a ring plane. This assumption is necessary as the orientation of the chemical shift tensor for various carbons in this banana molecule is unavailable. Initially, the biphenyl carbon chemical shifts were fitted at each temperature. The two ($S_{x'x'} - S_{y'y'}$) were found to depend linearly on temperature, while $S_{z'z'}$ followed the Haller equation:

TABLE 2: CSA Tensors for Other Carbon Sites (Site Labels Are for Both *Lateral* Wings)

sites	2[a]	3[b]	4[a]	5[b]	8[c]
δ_{11}	8.7	21.8	14.6	20	8.7
δ_{22}	135.5	145.5	147.4	173	155.7
δ_{33}	192.6	217.9	219.3	236	227.7
δ_{iso}	112.2	128.4	127.1	143	130.7

[a] Reference 49. [b] Reference 50. [c] Reference 51.

$$S_{z'z'}(T) = S_0(1 - T/T^*)^f \quad (3)$$

where S_0 and f are empirical constants and T^* is the temperature slightly above T_c at which $S_{z'z'}$ becomes zero. In the global analysis, the above equation was used to describe the local order parameter $S_{z'z'}(T)$ with $T^* = T_c + 1$ K. A linear equation was used to describe the temperature dependence of ($S_{x'x'} - S_{y'y'}$), i.e., $S_{x'x'} - S_{y'y'} = S_\Delta(T - T_c)$ where S_Δ is a fitting constant.

The same procedures were used for the carbon sites 10 and 12 to give local order parameters S_{zz} and $S_{xx} - S_{yy}$.

The calculated chemical shifts for fitted carbon sites are shown as solid lines in Figure 8, and the S_{zz} values of central ring and $S_{z'z'}$ values of biphenyl groups obtained from the fittings are shown in Figure 9a with S_0 and f for the biphenyl group and central ring being (0.76, 0.15) and (0.92, 0.17), respectively. Figure 9b shows the linear temperature behaviors of ($S_{xx} - S_{yy}$) and two ($S_{x'x'} - S_{y'y'}$) for the two biphenyl rings. Now our results imply that the local z axis located on the central ring represents a more ordered axis (or the long molecular axis), and thus reflects the overall molecular ordering. The z' axis along the para axes in the biphenyl group is less ordered. Indeed, S_{zz} is found similar to that reported for the nematic order parameter,[15] and varies between 0.36 and 0.6 in the nematic range. Now one can use the following approximate equation[52] to relate the ordering of these local z axes

$$S_{z'z'} \approx S_{zz}P_2(\cos\theta) \quad (4)$$

where θ is the angle between the para axes of a biphenyl group (z' axis) and the more ordered axis (z axis). Using this equation, an average angle $\theta \approx 15.67$ is estimated, which is slightly larger than the value of 11.8° found in the banana mesogen ClPbis11BB. Hence, the average bending angle subtended by the two lateral arms in 10DClPBBC is determined to be 148.7° in the present study. This angle is larger than monosubstituted chlorine banana mesogens.[15] The ($S_{x'x'} - S_{y'y'}$) found for the outer ring in a biphenyl group is slightly less than that of the ring closer to the central ring (Figure 9b). In general, the local biaxial orders of the fragments are relatively small, and their magnitudes are perhaps less certain due to inaccurate CSA for some carbon sites (e.g., Table 2). For the central ring, ($S_{xx} - S_{yy}$) is about 0.05 at 64.5 °C and becomes zero near T_c.

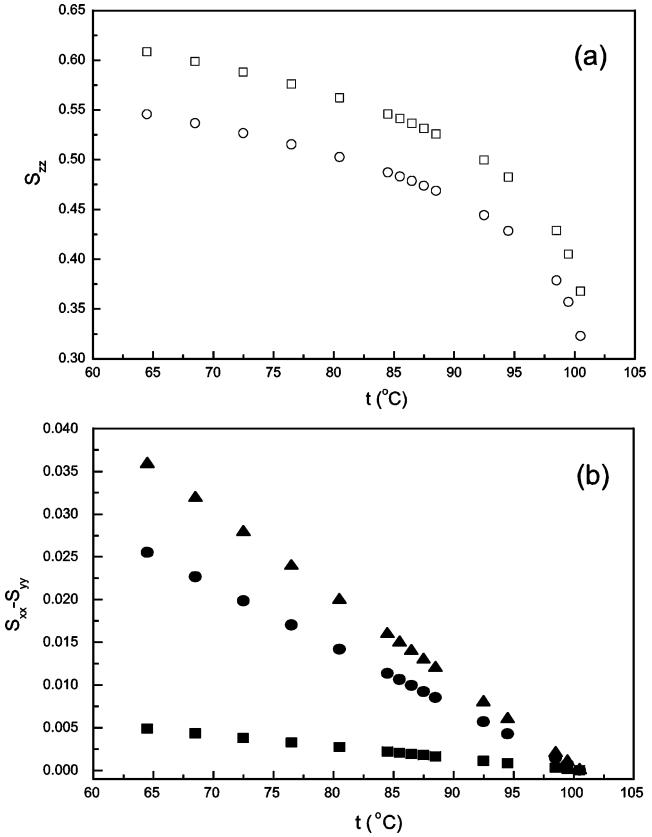

Figure 9. (a) Plot of the local order parameter S_{zz} for the biphenyl group (○) and central ring (□) in the nematic phase of 10DClPBBC. (b) Plot of the local biaxial order parameter ($S_{xx} - S_{yy}$) vs temperature (▲ is central ring; ● is for the ring closer to the central ring; ■ is for the outer biphenyl ring)

The local order tensors of phenyl rings in the biphenyl fragment can also be studied at 78 °C using the dipolar oscillations due to C−H dipolar couplings seen in the SLF experiment. The observed C−H dipolar splittings $\Delta\nu_{ij}$ (between the outer peaks) in Figure 7 can be understood using[33]

$$\Delta\nu_{ij} = f(2D_{ij} + J_{ij}) \tag{5}$$

where f is the scaling factor of the dipolar decoupling sequence, J_{ij} is the C−H scalar coupling constant (assumed to be negligible), and D_{ij}, the C−H dipolar coupling constant, is given by

$$D_{ij} = -(k_{ij}/r_{ij}^3)\Big[P_2(\cos\theta_{z'}^{ij})S_{z'z'} + \frac{1}{2}(\cos^2\theta_{x'}^{ij} - \cos^2\theta_{y'}^{ij})(S_{x'x'} - S_{y'y'})\Big] \tag{6}$$

with $k_{ij} = 30.74$ kHz Å^3 for a bonded C−H spin pair, θ_α^{ij} is the angle between the internuclear ij vector (r_{ij}) and the α axis of the local (x', y', z') frame. We have chosen $r_{CH} = 1.09$ Å and $r_{CC} = 1.4$ Å. For the ortho and meta carbons on the phenyl ring, one has to consider both $\Delta\nu_1$ due the attached proton and $\Delta\nu_2$ due the nearby nonbonded proton (e.g., for carbon 2, the former is due to H(2) and the latter is due to H(3) where the number inside the parentheses denotes the carbon number to which the proton is attached). The observed dipolar splitting is then given by $\sqrt{(\Delta\nu_1)^2+(\Delta\nu_2)^2}$. For the quaternary carbons, the two nonbonded protons are located at the same r_{ij} making the observed splitting being given by $\sqrt{2}\ \Delta\nu_{ij}$.[37] For each phenyl ring, one has four observed dipolar splittings (tabulated in Table 3) from which two unknowns $S_{z'z'}$ and ($S_{x'x'} - S_{y'y'}$) can be determined using eq 5. To determine the local order tensors for the two phenyl rings keeping $S_{z'z'}$ the same, we have chosen to optimize the ring geometry. For the outer phenyl ring, we found that $\theta_{z'}^{CH} = 58.5°$ and 59° for sites 2 and 3, respectively, and $S_{z'z'} = 0.52$ and ($S_{x'x'} - S_{y'y'}$) = 0.07, whereas for the other ring in the biphenyl fragment $\theta_{z'}^{CH} = 60°$ (not varied) for site 6 and 59.3° for site 7, and $S_{z'z'} = 0.52$ and ($S_{x'x'} - S_{y'y'}$) = 0.05. In this calculation, six target parameters were varied to best fit the experimental splittings in Table 3. The calculated splittings are also listed in this table. The agreement between calculated and experimental splittings is good except for sites 5 and 8. This could be attributed to their weaker broad lines. The local $S_{z'z'}$ value found here appears to be consistent with the corresponding local $S_{z'z'}$ value (0.51) found from the global analysis of ^{13}C chemical shift data of biphenyl group at the same temperature. The local molecular biaxialities of the two rings appear tbe quite similar in view of uncertain geometry, but seem slightly larger than those given above at this temperature. The distortion in $\theta_{z'}^{CH}$ from the nominal 60° value could partly due to the inaccurate determination of dipolar couplings resulting from relatively broad lines seen in the SLF experiment.

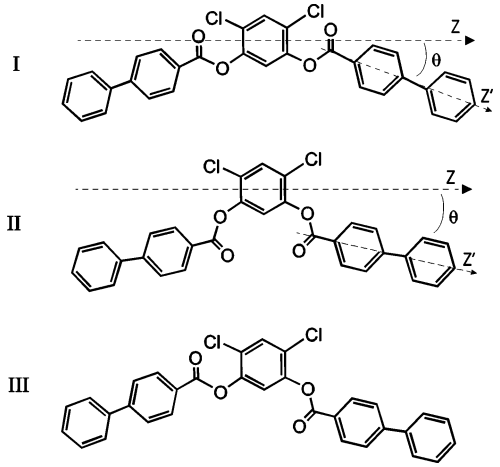

Figure 10. Some probable configurations of the studied banana core (see text).

TABLE 3: Dipolar Splittings of Biphenyl Fragment from SLF Experiment

sites	expt splittings/sinθ_m (kHz)	calcd splittings $2D_{ij}$ (kHz)
1	2.55 ± 0.02	2.54
2	4.05 ± 0.01	4.04
3	4.27 ± 0.01	4.27
4	2.51 ± 0.02	2.52
5	2.54 ± 0.11	2.41
6	4.58 ± 0.01	4.57
7	4.21 ± 0.01	4.22
8	2.30 ± 0.05	2.44

The present analyses do not require specific motional processes (internal and external motions of the banana core), or need to know its particular core conformation. Indeed, there may be several possible configurations generated by a rotation of the lateral arm about the C_{ar}−C bond at the central ring as depicted in Figure 10. The $S_{z'z'}$ is less than S_{zz} partly due to the molecular structure of a particular conformation, and partly due to possible "fast" conformational transitions among different available configurations. Even if there are more than one stable configuration, the conformational changes are fast on the NMR time scale such that a simple ^{13}C spectrum is obtained at a particular temperature. If this is not the case, different subspectra

would be visible in the observed spectrum just like the doubling of the ^{13}C peaks seen in a monosubstituted analogue 11ClPBBC.[15] Finally, the angle θ in eq 4 may be interpreted as some configurational average angle between the two differently ordered axes in this banana core. The question of exactly how many (if any) conformations and their structures as well as their probabilities in the nematic potential for a relatively large molecule remains open. However, based on the quantum chemical calculations of a similar compound ClPbis11BB[16] and the above θ value, the predominant core configuration is likely the conformer II shown in Figure 10.

Conclusion

The present study has demonstrated how 2D ^{13}C NMR can play an important role in the study of structures and orientational order in banana mesogens. In particular, the SUPER experiment can be employed to give more precise magnitudes of principal elements in CSA tensors for the particular liquid crystal in question. This particular 2D MAS technique has not been applied to liquid crystals until now. Although 2D-PASS has been used in liquid crystals, we have found that the implementation of the SUPER method seems to be easier. The other 2D NMR techniques are useful to confirm of ^{13}C peak assignments in the 1D proton-decoupled ^{13}C spectrum. The present study has enabled us to get the order parameters of the central ring. In addition, the average bending angle subtended by the two arms of the bent-core structure in 10DClPBBC is found to be 148.7°.

Acknowledgment. The financial support of Natural Sciences and Engineering Council of Canada and Brandon University are gratefully acknowledged. We thank the Canada Foundation of Innovation for the NMR facility, and Mr. N. Finlay for his technical support. K.F.C. is grateful to OTKA for the financial support.

References and Notes

(1) Dong, R. Y. Advances in NMR studies of liquid crystals. *Annu. Rep. NMR Spectrosc.* **2004**, *53*, 68.

(2) Burnell, E. E.; Delange, C. A. *NMR of Ordered Liquids*; Kluwer: Dordrecht, The Nehterlands, 2003.

(3) Niori, T.; Sekine, F.; Watanabe, J.; Furukawa, T.; Taklzoe, H. *J. Mater. Chem.* **1996**, *7*, 1231.

(4) Pelzl, G.; Diele, S.; Weissflog, W. *Adv. Mater.* **1999**, *11*, 707.

(5) Link, D. R.; Natale, G.; Shao, R.; Maclennan, J. E.; Clark, N. A.; Körblova, E.; Walba, D. M. *Science* **1997**, *278*, 1924.

(6) Eremin, A.; Wirth, I.; Diele, S.; Pelzl, G.; Schmalfuss, H.; Kresse, H.; Nadasi, H.; Fodor-Csorba, K.; Gacs-Baitz, E. W. *Liq. Cryst.* **2002**, *29*, 775.

(7) Madsen, L. A.; Dingemans, T. J.; Nakata, M.; Samulski, E. T. *Phys. Rev. Lett.* **2004**, *92*, 145505.

(8) Acharya, B. R.; Primak, A.; Kumar, S. *Phys. Rev. Lett.* **2004**, *92*, 145506.

(9) Hughes, J. R.; Kothe, G.; Luckhurst, G. R.; Malthête, J.; Neubert, M. E.; Shenouda, I.; Timimi, B. A.; Tittelbach, M. *J. Chem. Phys.* **1997**, *107*, 9252.

(10) Kurosu, H.; Kawasaki, M.; Hirose, M.; Yamada, M.; Kang, S.; Thisayukta, J.; Sone, M.; Takezoe, H.; Watanabe, J. *J. Phys. Chem. A* **2004**, *108*, 4674.

(11) Weissflog, W.; Lischka, C.; Diele, S.; Pelzl, G.; Wirth, I.; Grande, S.; Kresse, H.; Schmalfuss, H.; Hartung, H. *Mol. Cryst. Liq. Cryst.* **1999**, *333*, 203.

(12) Diele, S.; Grande, S.; Kruth, H.; Lischka, Ch.; Pelzl, G.; Weissflog, W.; Wirth, I. *Ferroelectrics* **1998**, *212*, 169.

(13) Pelzl, G.; Grande, S.; Jakli, A.; Lischka, Ch.; Kresse, H.; Schmalfuss, H.; Wirth, I.; Weissflog, W. *Liq. Cryst.* **1999**, *26*, 401.

(14) Dehne, H.; Potter, M.; Sokolowski, S.; Weissflog, W.; Diele, S.; Pelzl, G.; Wirth, I.; Kresse, H.; Schmalfuss, H.; Grande, S. *Liq. Cryst.* **2001**, *28*, 1269.

(15) Dong, R. Y.; Xu, J.; Fodor-Csorba, K.; Gacs-Baitz, E. *Phys. Rev. E* **2004**, *79*, 011708.

(16) Dong, R. Y.; Fodor-Csorba, K.; Xu, J.; Domenici, V.; Prampolini, G.; Veracini, C. A. *J. Phys. Chem. B* **2004**, *108*, 7694.

(17) Nadasi, H.; Weissflog, W.; Eremin, A.; Pelzl, G.; Diele, S.; Das, B.; Grande, S. *J. Mater. Chem.* **2002**, *12*, 1316.

(18) Grant, D. M. Chemical shift Tensors. In *Encyclopedia of Nuclear Magnetic Resonance*; Wiley: New York, 1996; p 1298.

(19) Maricq, M. M.; Waugh, J. S. *J. Chem. Phys.* **1979**, *70*, 3300.

(20) Herzfeld, J.; Berger, A. E. *J. Chem. Phys.* **1980**, *73*, 6021.

(21) Schmitdt-Rohr, K.; Spiess, H. W. *Multidimensional Solid-State NMR and Polymers*; Academic Press: London 1994.

(22) Tycko, R.; Dallagh, G.; Mirau, P. *J. Magn. Reson.* **1989**, *85*, 265.

(23) Hodgkinson, P.; Emsley, L. *J. Chem. Phys.* **1997**, *107*, 4808.

(24) Antzutkin, O. N.; Shekar, S. C.; Levitt, M. H. *J. Magn. Reson. A* **1995**, *115*, 7.

(25) Dollase, W. A.; Feike, M.; Förster, H.; Schaller, T.; Schnell, I.; Sebald, A.; Steuernage, S. *J. Am. Chem. Soc.* **1997**, *119*, 3807.

(26) Liu, S−F.; Mao, J.-D.; Schmidt-Rohr, K. *J. Magn. Reson.* **2002**, *155*, 15.

(27) Bielecki, A.; Burum, D. P.; Rice, D. M.; Karasz, F. E. *Macromolecules* **1991**, *24*, 4820.

(28) van Rossum, B.-J.; Förster, H.; de Groot, H. J. M. *J. Magn. Reson.* **1997**, *124*, 516.

(29) Lesage, A.; Emsley, L. *J. Magn. Reson.* **2001**, *148*, 449.

(30) Opella, S. J.; Waugh, J. S. *J. Chem. Phys.* **1977**, *66*, 4919.

(31) Hester, R. K.; Ackerman, J. L.; Neff, B. L.; Waugh, J. S. *Phys. Rev. Lett.* **1976**, *36*, 1081.

(32) Dvinskikh, S. V.; Zimmermann, H.; Maliniak, A.; Sandstrom, D. *J. Magn. Reson.* **2003**, *163*, 46.

(33) Fung, B. M.; Ermolaev, K.; Yu, Y. *J. Magn. Reson.* **1999**, *138*, 28.

(34) Caldarelli, S.; Hong, M.; Emsley, L.; Pines, A. *J. Phys. Chem.* **1996**, *100*, 18696.

(35) Hong, M.; Caldarelli, S.; Schmidt-Rohr, K.; Pines, A. *J. Phys. Chem.* **1996**, *100*, 14815.

(36) Caldarelli, S.; Lesage, A.; Emsley, L. *J. Am. Chem. Soc.* **1996**, *118*, 12224.

(37) Nagaraja, C. S.; Ramanathan, K. V. *Liq. Cryst.* **1999**, *26*, 17.

(38) Fodor-Csorba, K.; Vajda, A.; Jakli, A.; Slugovc, C.; Trimmel, G.; Demus, D.; Gacs-Baitz, E.; Holly, S.; Galli, G. *J. Mater. Chem.* (submitted).

(39) Fung, B. M.; Khitrin, A. K.; Ermolaev, K. *J. Magn. Reson.* **2000**, *142*, 97.

(40) Tycko, R.; Dabbagh, G.; Mirau, P. A. *J. Magn. Reson.* **1989**, *85*, 265.

(41) deAzevedo, E. R.; Hu, W.-G.; Bonagamba, T. J.; Schmidt-Rohr, K. *J. Chem. Phys.* **2000**, *112*, 8988.

(42) States, D. J.; Haberkorn, R. A.; Ruben, D. J. *J. Magn. Reson.* **1982**, *48*, 286.

(43) Bielecki, A.; Kolbert, A. C.; Levitt, M. H. *Chem. Phys. Lett.* **1989**, *155*, 341 Bielecki, A.; Kolbert, A. C.; de Groot, H. J. M.; Griffin, R. G.; Levitt, M. H. *Adv. Magn. Reson.* **1990**, *14*, 111.

(44) Lee, M.; Goldburg, W. *Phys. Rev.* **1965**, *140*, A1261.

(45) Wu, C. H.; Ramamoorthy, A.; Opella, S. J. *J. Magn. Reson. A* **1994**, *109*, 270.

(46) Sinha, N.; Ramanathan, K. V. *Chem. Phys. Lett.* **2000**, *332*, 125.

(47) Eichele, K.; Wasylishen, R. WSOLIDS1 v. 1. 17.34, Dalhousie University, 2001.

(48) Wemmer, E.; Pines, A. *J. Am. Chem. Soc.* **1981**, *103*, 34.

(49) Zheng, G.; Hu, J.; Zhang, X.; Shen, L.; Ye, C.; Webb, G. A. *J. Mol. Struct. (THEOCHEM)* **1998**, *428*, 283.

(50) Nakai, T.; Fujimori, H.; Kuwahara, D.; Miyajima, S. *J. Phys. Chem. B* **1999**, *103*, 417.

(51) Wemmer, D. E.; Pines, A.; Whitehurst, D. D. *Philos. Trans. R. Soc. London A* **1981**, *300*, 15.

(52) Catalano, D.; Cavazza, M.; Chiezzi, L.; Geppi, M.; Veracini, C. A. *Liq. Cryst.* **2000**, *27*, 621.